Soft Matter

PAPER

Cite this: *Soft Matter*, 2019, **15**, 331

Stress-dependent amplification of active forces in nonlinear elastic media

Pierre Ronceray,[a] Chase P. Broedersz[b] and Martin Lenz*[cd]

Received 9th May 2018,
Accepted 10th December 2018

DOI: 10.1039/c8sm00949j

rsc.li/soft-matter-journal

The production of mechanical stresses in living organisms largely relies on localized, force-generating active units embedded in filamentous matrices. Numerical simulations of discrete fiber networks with fixed boundaries have shown that buckling in the matrix dramatically amplifies the resulting active stresses. Here we extend this result to a continuum elastic medium prone to buckling subjected to an arbitrary external stress, and derive analytical expressions for the active, nonlinear constitutive relations characterizing the full active medium. Inserting these relations into popular "active gel" descriptions of living tissues and the cytoskeleton will enable investigations into nonlinear regimes previously inaccessible due to the phenomenological nature of these theories.

I. Introduction

Cells move and deform in response to stresses. These stresses originate both from the deformation of their environment, and from the active forces they generate internally. Within the cell, these forces are largely generated by molecular motors acting at the nanometer scale that are embedded in a matrix of semi-flexible filaments known as the actin cytoskeleton. The cytoskeleton then transmits these forces to larger length scales, allowing them to control shape and generate stresses over the whole cell. At even larger length scales, the resulting cell-wide forces can be further transmitted by another type of fibrous network, the extracellular matrix, and this transmission results in stress production over several millimeters in connective tissues.[1] Much progress has been made recently in understanding how these active forces are transmitted by fiber networks from the microscopic to macroscopic scales, thus enabling cell motion and division, wound healing or embryonic development.[2,3] Furthermore, it is now well understood how passive biopolymer networks, both inside and outside cells, respond to external strain.[4] However, little is known about the interplay between internal stress generation and external stresses due to environment strain.

The key to a theory of stress generation in fiber networks is understanding how they transmit forces from small to large scales. While the quantitative relationship between microscopic forces and the resulting macroscopic stresses is remarkably simple in linear elastic media,[5,6] this force transmission is drastically modified by the nonlinear response conferred to fibrous media by the buckling of their filaments.[7–12] Quantitatively, there the tensile stress σ_{active} actively generated by a density ρ of active units each exerting a force dipole D can exceed the linear prediction

$$\sigma_{\text{active}}^{(\text{lin})} = -\rho D \tag{1}$$

by several orders of magnitude. Qualitatively, strong active units locally deform the networks and thus surround themselves with a potentially large buckled region, where the network is mechanically equivalent to a collection of tense radial ropes. Such stress propagation patterns are described by the general mathematical formalism of tension field theory,[13,14] and are also encountered in thin, easily buckled elastic sheets.[15] As the ropes transmit the forces produced by the active unit to the boundary of that buckled region, the system comprised of the active unit plus the ropes acts like an enlarged, effective force dipole. This effective dipole has an enhanced span compared to the original one, and thus a larger magnitude $|D^{\text{eff}}| > |D|$ (Fig. 1). However, how external strain affects stress generation and modifies these scaling laws is not known. Moreover, a detailed analytical understanding of buckling-induced stress amplification is missing, although other types of nonlinearities have been investigated in two dimensions.[7,11]

In this paper, we demonstrate that the effect of external stress on active stress generation can be simply understood as an enhancement of the buckling threshold. To this aim, we derive a full analytical description of active stress amplification in a simple model of bucklable medium subjected to an arbitrary external isotropic stress in any dimension. We restrict our study to isotropic, contractile active units, motivated by the observation that they represent the generic far-field response of a fiber

[a] *Princeton Center for Theoretical Science, Princeton University, Princeton, NJ 08544, USA*
[b] *Arnold-Sommerfeld-Center for Theoretical Physics and Center for NanoScience, Ludwig-Maximilians-Universität München, D-80333 München, Germany*
[c] *LPTMS, CNRS, Univ. Paris-Sud, Université Paris-Saclay, 91405 Orsay, France. E-mail: martin.lenz@u-psud.fr*
[d] *MultiScale Material Science for Energy and Environment, UMI 3466, CNRS-MIT, 77 Massachusetts Avenue, Cambridge, Massachusetts 02139, USA*

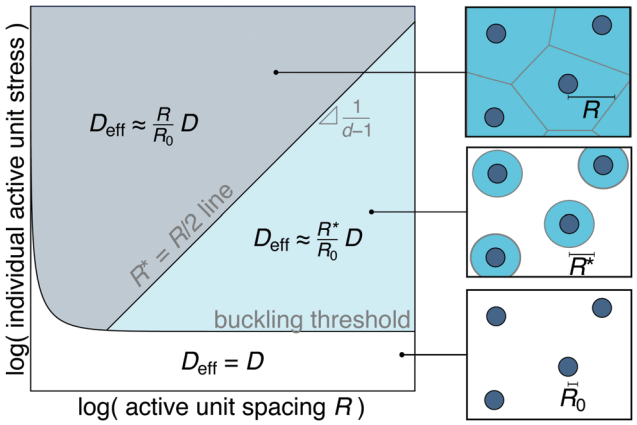

Fig. 1 A medium populated by strong enough contractile active units (dark blue) buckles and amplifies their active stresses. The phase diagram on the left delimits three buckling regimes, whose physical structures are illustrated by panels on the right. White regime: weak active units do not induce buckling, yielding a far-field stress given by eqn (1). Blue regime: stronger active units locally buckle the network by exerting compressive stresses in excess of the buckling threshold σ_b. This endows each active unit with a larger effective dipole $D_{\rm eff} \approx (R^*/R_0)D$, where R^* is the radius of the light blue buckled region and R_0 that of an active unit. Grey regime: for a medium with fixed boundary, the buckling radius asymptotically goes to the distance R between active units as the strength of the active units becomes very large, implying that $D_{\rm eff} \approx (R/R_0)D$. In this work we show that imposing an external stress σ at the boundary of the medium modifies the values of $D_{\rm eff}$ and R^* in the same way as a shift of the buckling threshold from σ_b to $\sigma_b + \sigma$.

network to any large local force dipole, be it locally contractile or extensile, isotropic or anisotropic.[12] We present the ingredients of our model in Section II, and compute the characteristics of the forces transmitted by our active medium in Section III. We then deduce the resulting macroscopic stresses in Section IV, and use these expressions to derive constitutive stress–strain relations for the active medium in Section V. Finally, we discuss our results in Section VI.

The analytical expressions derived here are key to incorporating the wealth of available biological and mechanical information about individual active units in so-called active gel theories, which are widely used theoretical descriptions of living tissues and the cytoskeleton.[16–18] Indeed, such theories typically adopt a purely macroscopic point of view, and while active stresses are the fundamental drivers of the new physics they explore, active gel descriptions typically assume them to be constant for lack of a better description.[19]

II. Model

Our aim is to model a fiber network subject to stresses that are both externally applied and induced internally by active units. To this end, we consider a homogeneous nonlinear medium in spatial dimension d (with $d = 2$ or 3 in practice) subjected to an isotropic external stress σ, and within which a density ρ of active units are embedded. Assuming for simplicity that the active units are positioned on a regular lattice (*e.g.*, a triangular lattice in 2D), we focus on the Voronoi cell surrounding one of the active units (*e.g.*, a hexagon in a triangular lattice). We further approximate this cell by a spherical domain with the same volume as the Voronoi cell, allowing us to consider only spherically symmetric configurations in the following. The radius R of this sphere as a function of the motor density is set by $\rho S_{d-1} R^d = 1$, with S_n the volume of the unit n-sphere ($S_1 = \pi$, $S_2 = 4\pi/3$).

To account for fiber buckling, the continuum elastic medium can locally buckle when compressed beyond a critical stress σ_b. To implement this feature in the simplest fashion, we assume that the medium responds linearly with Lamé coefficients λ and μ, but that compressive stresses saturate beyond the threshold value $-\sigma_b$. To express this relation formally, we denote the strain and stress tensors by $\boldsymbol{u}$ and $\boldsymbol{\sigma}$ respectively, and note that the spherical symmetry of the system imposes that both tensors take a diagonal form in spherical coordinates, resulting in the following block structure:

$$\boldsymbol{u} = \begin{pmatrix} u_{rr} & 0 \\ 0 & u_{\theta\theta} I \end{pmatrix} \quad \text{and} \quad \boldsymbol{\sigma} = \begin{pmatrix} \sigma_{rr} & 0 \\ 0 & \sigma_{\theta\theta} I \end{pmatrix}, \tag{2}$$

where I is the $(d-1)$-dimensional unit matrix. In this simple geometry, the radial and orthoradial stresses in the linear regime read

$$\sigma_{rr}^{\rm lin} = (\lambda + 2\mu) u_{rr} + (d-1)\lambda u_{\theta\theta} \tag{3a}$$

$$\sigma_{\theta\theta}^{\rm lin} = \lambda u_{rr} + [(d-1)\lambda + 2\mu] u_{\theta\theta}, \tag{3b}$$

and our buckling condition can be formulated as

$$\begin{aligned} &\text{if } \sigma_{rr}^{\rm lin} > -\sigma_b \quad \text{and} \quad \sigma_{\theta\theta}^{\rm lin} > -\sigma_b, \quad \text{then} \begin{cases} \sigma_{rr} = \sigma_{rr}^{\rm lin} \\ \sigma_{\theta\theta} = \sigma_{\theta\theta}^{\rm lin} \end{cases} \\ &\text{if } \sigma_{rr}^{\rm lin} < -\sigma_b, \quad \text{then } \sigma_{rr} = -\sigma_b \\ &\text{if } \sigma_{\theta\theta}^{\rm lin} < -\sigma_b, \quad \text{then } \sigma_{\theta\theta} = -\sigma_b, \end{aligned} \tag{4}$$

where $\sigma_b \geq 0$. Note that we do not need to make specific assumptions about the strain dependence of σ_{rr} when $\sigma_{\theta\theta}^{\rm lin} < -\sigma_b$ (or that of $\sigma_{\theta\theta}$ when $\sigma_{rr}^{\rm lin} < -\sigma_b$) for the purpose of this study, since these components of the stress are then fully determined by force balance. In particular, eqn (4) neither assumes nor discounts the possibility that the medium stiffens under uniaxial stretching once driven into the nonlinear regime.

The elastic medium is centred around an active unit, consisting of a sphere of radius $R_0 < R$ imposing a contractile stress $\sigma_0 > 0$ [Fig. 2(a)]. This geometry yields a stress discontinuity at the surface of the active unit

$$\lim_{\varepsilon \to 0} [\sigma_{rr}(R_0 + \varepsilon) - \sigma_{rr}(R_0 - \varepsilon)] = \sigma_0. \tag{5}$$

Defining the force dipole exerted by a spatial distributions $f_i(\mathbf{r})$ of body forces as $D_{ij} = \int r_i f_j(\mathbf{r}) \mathrm{d}\mathbf{r}$, our spherically symmetric dipole reads $D_{ij} = D\delta_{ij}$ with $D = -S_{d-1}\sigma_0 R_0^d$. The presence of the elastic medium within our active unit is theoretically convenient in two respects. It guarantees that the $\sigma_0 \to 0$ limit corresponds to a passive, homogeneous active medium, and ensures that dipole conservation in the linear regime is expressed as the compact

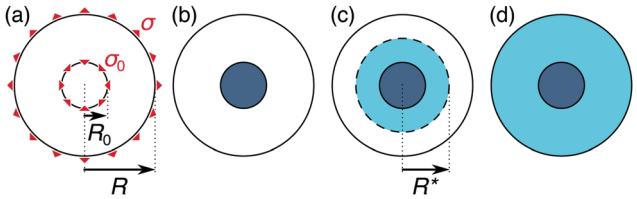

Fig. 2 Successive buckling states of the elastic medium. Red arrowheads on the first panel picture the active internal compression applied across the $r = R_0$ circle, as well as the tensile boundary stress σ. White regions are in the linear regime in both the radial and orthoradial directions in the sense of eqn (4). Light blue regions are buckled in the orthoradial directions only, and dark blue regions are buckled in both directions. Qualitatively, as the active unit generates a strong local compressive stress at the center of the medium, buckling is initiated there, then progresses outwards as the active unit stress σ_0 is increased. A large value of the tensile prestress σ antagonizes this compression, delays buckling and hinders the amplification of active stresses.

condition of eqn (1).[6] This feature is additionally relevant to an experimental situation where, *e.g.*, a long thin myosin thick filament embedded in an actin network binds two actin fibers at its end points and compresses the network between these two points. Similarly, a flattened contractile cell deposited onto an elastic sheet imposes an in-plane compression on the piece of the sheet that it covers. Removing this inner piece of medium slightly modifies our results, as it implies a softening of the overall medium and a slight reinforcement of the apparent contractile stress without any qualitative change in our conclusions.

We further assume that the elastic medium is held under constant stress $\sigma_{ij} = \sigma\delta_{ij}$ at its outer boundary, implying the boundary condition

$$\sigma_{rr}(R) = \sigma, \tag{6}$$

where this external stress σ may be positive or negative.

To compute the stress and displacements associated with our active unit, we must solve the mechanical equilibrium equations $\nabla_j\sigma_{ij} = 0$ for our elastic medium, which in our spherical geometry reads

$$\frac{1}{r^{d-1}}\frac{\mathrm{d}\left(r^{d-1}\sigma_{rr}\right)}{\mathrm{d}r} - \frac{(d-1)\sigma_{\theta\theta}}{r} = 0, \tag{7}$$

where σ_{rr} and $\sigma_{\theta\theta}$ are related to the strain by eqn (4). We can furthermore express the strain as a function of the radial displacement $u(r)$ of the elastic medium through

$$u_{rr}(r) = \mathrm{d}u/\mathrm{d}r \tag{8a}$$

$$u_{\theta\theta}(r) = u/r. \tag{8b}$$

Finally, $u(0) = 0$ due to spherical symmetry.

III. Buckling transitions

Depending on the values of σ and σ_0, our elastic medium undergoes a sequence of buckling transitions, as illustrated in Fig. 2. In the following we completely characterize this sequence for non-auxetic materials, *i.e.* materials with a positive Poisson ratio, or equivalently a positive λ.

For low active unit stresses σ_0, the material responds linearly [Fig. 2(a)], and we supplement eqn (3)–(8) with the requirement that $u(r)$ be continuous in R_0. This yields

$$u(r<R_0) = \left\{\frac{\sigma}{d\lambda+2\mu} - \frac{\sigma_0}{d(\lambda+2\mu)} \times\left[1+\frac{2\mu(d-1)}{d\lambda+2\mu}\left(\frac{R_0}{R}\right)^d\right]\right\}r \tag{9a}$$

$$u(r>R_0) = \left[\frac{\sigma}{d\lambda+2\mu} - \frac{2\mu(d-1)\sigma_0}{d(\lambda+2\mu)(d\lambda+2\mu)}\left(\frac{R_0}{R}\right)^d\right]r - \frac{\sigma_0}{d(\lambda+2\mu)}\frac{R_0^d}{r^{d-1}}. \tag{9b}$$

Increasing the active unit strength σ_0 from this linear regime puts the $r < R_0$ region under an increasing isotropic compressive stress. As this compressive stress reaches the $-\sigma_\mathrm{b}$ threshold for $\sigma_0 = \sigma_0^{\mathrm{buckling1}}$, with

$$\sigma_0^{\mathrm{buckling1}} = \frac{d(\lambda+2\mu)(\sigma+\sigma_\mathrm{b})}{d\lambda+2\mu+2\mu(d-1)(R_0/R)^d}, \tag{10}$$

the buckling regime of Fig. 2(b) sets in. In the central buckled region, eqn (4) then implies $\sigma_{rr}(r<r_0) = \sigma_{\theta\theta}(r<r_0) = -\sigma_\mathrm{b}$. Further solving eqn (3)–(8) in the region $R_0 < r < R$ where the medium responds linearly, we find

$$u(r>R_0) = \left[\frac{\sigma}{1-(R_0/R)^d} + \frac{\sigma_\mathrm{b}-\sigma_0}{(R/R_0)^d-1}\right]\frac{r}{d\lambda+2\mu} + \frac{\sigma+\sigma_\mathrm{b}-\sigma_0}{2\mu(d-1)\left(R_0^{-d}-R^{-d}\right)}\frac{1}{r^{d-1}}. \tag{11}$$

Upon a further increase of the active unit strength, the compressive orthoradial stress $\sigma_{\theta\theta}(R_0^+)$ at the outer surface of the active unit reaches the buckling threshold for $\sigma_0 = \sigma_0^{\mathrm{buckling2}}$, with

$$\sigma_0^{\mathrm{buckling2}} = \frac{d(\sigma+\sigma_\mathrm{b})}{1+(d-1)(R_0/R)^d}. \tag{12}$$

Beyond this threshold, the elastic medium buckles in the orthoradial direction in the region outside the active unit, as pictured in Fig. 2(c). We denote by R^* the outer limit of this buckling zone. In this regime, $\sigma_{rr}(r<R_0) = \sigma_{\theta\theta}(r<R^*) = -\sigma_\mathrm{b}$. Radial force balance additionally imposes that σ_{rr} be a continuous function in R^*, and the value of the buckling radius R^* is set by the buckling condition $\sigma_{\theta\theta}(R^*) = -\sigma_\mathrm{b}$. Solving eqn (3)–(8) while taking into account these new boundary conditions yields

$$\sigma_{rr}(R_0<r<R^*) = \sigma_0\left(\frac{R_0}{r}\right)^{d-1} - \sigma_\mathrm{b} \tag{13a}$$

$$u(r>R^*) = \frac{\sigma(R/R^*)^d+\sigma_\mathrm{b}-\sigma_0(R_0/R^*)^{d-1}}{(d\lambda+2\mu)\left[(R/R^*)^d-1\right]}r + \frac{\sigma+\sigma_\mathrm{b}-\sigma_0(R_0/R^*)^{d-1}}{2\mu(d-1)\left[(R^*)^{-d}-R^{-d}\right]}\frac{1}{r^{d-1}}, \tag{13b}$$

where R^* is the solution of the following equation:

$$\left(\frac{R^*}{R}\right)^d - \frac{d}{d-1}\frac{\sigma+\sigma_b}{\sigma_0}\left(\frac{R^*}{R_0}\right)^{d-1} + \frac{1}{d-1} = 0. \quad (14)$$

Eqn (14) implies that as long as the buckling zone is much smaller than the size of the entire system ($R^* \ll R$) its radius is given by

$$R^* = R_0\left[\frac{\sigma_0}{d(\sigma+\sigma_b)}\right]^{1/(d-1)}, \quad (15)$$

which confirms the scaling postulated in ref. 12. More broadly, in $d = 2$ the buckling radius is given by

$$R^*/R = \frac{(\sigma+\sigma_b)R}{\sigma_0 R_0} - \sqrt{\left[\frac{(\sigma+\sigma_b)R}{\sigma_0 R_0}\right]^2 - 1}, \quad (16a)$$

while in $d = 3$

$$\frac{2\sigma_0 R_0^2 R^*}{(\sigma+\sigma_b)R^3} = 1 - 2\cos\left\{\frac{1}{3}\arccos\left[\frac{2\sigma_0^3 R_0^6}{(\sigma+\sigma_b)^3 R^6} - 1\right] - \frac{2\pi}{3}\right\}. \quad (16b)$$

We plot both of these solutions in Fig. 3. Eqn (13a) confirms the observation made in ref. 12 that radial stresses decay slowly with a r^{1-d} power law within the $R_0 < r < R^*$ buckling region, thus accounting for long-range stress transmission in buckled systems, in contrast with the r^{-d} decay characteristic of linear materials. Throughout the regime described here, the buckling zone is under strong radial tensile stress, while it is essentially crumpled in the orthoradial direction, implying that $\sigma_{\theta\theta}$ provides little help in stabilizing the system against the radial tension. As a result, the buckling zone is prevented from collapsing primarily by the unbuckled shell surrounding it, which we picture in white in Fig. 2(c).

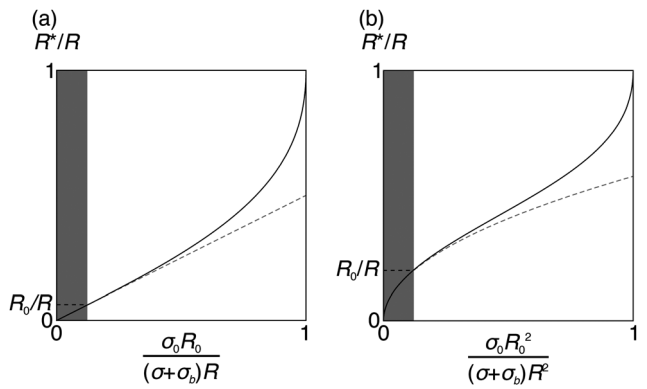

Fig. 3 Buckling radii characterizing the buckling regime of Fig. 2(c) in (a) $d = 2$ and (b) $d = 3$ as given by eqn (14) (solid black line) along with the asymptotic expression of eqn (15) (dashed gray line). The region of the curve corresponding to $R^* < R_0$ (gray box) is not relevant, as it corresponds to an active unit stress $\sigma_0 < \sigma_0^{\text{buckling2}}$, and thus to another buckling regime. Changes in the value of R_0/R result in a displacement of the boundary of the gray box, while the black curve is unaffected.

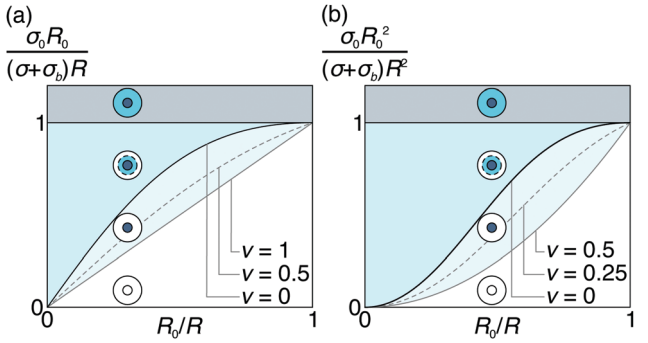

Fig. 4 Parameter values characterizing the four possible buckling regimes in dimensions (a) $d = 2$ and (b) $d = 3$. The lines on the diagrams are the boundaries of the different regimes. The position of the lower line (in grey) depends on the Poisson ratio $\nu = (d - 1 + 2\mu/\lambda)^{-1}$ of the material, and its position is indicated for three values of ν on each panel. In particular, for $\nu = 0$ this line is identical to the central black line and the second buckling regime of Fig. 2 is thus nonexistent. Note that thermodynamic stability requires $\nu \leq 1$ in $d = 2$ and $\nu \leq 0.5$ in $d = 3$.

As the active unit stress σ_0 is increased yet again, the buckling radius R^* reaches the boundary of the system for $\sigma_0 = \sigma_0^{\text{collapse}}$, with

$$\sigma_0^{\text{collapse}} = (\sigma+\sigma_b)\left(\frac{R}{R_0}\right)^{d-1}. \quad (17)$$

Beyond this value, the stabilizing unbuckled outer shell vanishes and the system collapses. Formally, this collapse is manifested by the mechanical equilibrium equation eqn (7) having no solution that satisfies both boundary conditions eqn (5) and (6).

We illustrate the parameter ranges associated with the four buckling regimes discussed in this section in the phase diagram of Fig. 4.

IV. Stress amplification

The external stress σ applied at the boundary of the elastic medium is balanced by two contributions: a passive elastic response of the network, and an active stress specifically due to the presence of these active units

$$\sigma = \sigma_{\text{elastic}} + \sigma_{\text{active}}, \quad (18)$$

This decomposition of total stress into a passive and an active contribution is a central ingredient of active gel theories,[6,16] where the contribution of σ_{active} drives nonequilibrium flows and pattern formation.[17,18,20–22] To determine σ_{active}, we determine σ_{elastic} as the stress that would be required to impose the same boundary displacement observed in our system onto a purely passive, $\sigma_0 = 0$ medium. Thus,

$$\sigma_{\text{elastic}} = (d\lambda + 2\mu)\frac{u(R)}{R} \quad (19)$$

Note that the previously studied special case of a fixed boundary corresponds to $\sigma_{\text{elastic}} = 0$.[12] Here we combine the displacements computed in Section III with eqn (18) and (19) to compute the dependence of the two stress contributions on the parameters of our model.

For a completely homogeneous linear (but possibly anisotropic) network, general linear elastic considerations[5,6] impose that the active stress is proportional to the force dipole and density of active units through $\sigma_{\text{active}}^{(\text{lin})} = -\rho D$. Indeed, combining eqn (9) with eqn (18) and (19) yields

$$\sigma_{\text{active}}^{(\text{lin})} = \sigma_0 \left(\frac{R_0}{R}\right)^d = -\rho D. \tag{20}$$

When active units are strong enough to buckle the network, the reference active stress of eqn (20) is amplified, which we quantify through the amplification factor

$$\mathcal{A} = \frac{\sigma_{\text{active}}}{\sigma_{\text{active}}^{(\text{lin})}}. \tag{21}$$

Combining the displacements of eqn (11) and (13b) with eqn (18) and (19) thus yields

$$\mathcal{A} = \frac{(\lambda + 2\mu)d}{2\mu(d-1)} \frac{1}{1-(R_0/R)^d}\left(1 - \frac{\sigma + \sigma_{\text{b}}}{\sigma_0}\right) \tag{22}$$

for the inner buckling regime illustrated in Fig. 2(b) and

$$\mathcal{A} = \left(1 + \frac{\lambda}{2\mu}\right)\frac{R^*}{R_0} \tag{23}$$

for the regime of Fig. 2(c). This last relationship validates the $\mathcal{A} \propto R^*/R_0$ scaling postulated for the "force-controlled" regime of ref. 12 on the basis of the amplified force dipole picture described in the introduction. Finally, no amplification factor can be computed for the collapsing regime of Fig. 2(d) as it does not give rise to a well-defined boundary displacement $u(R)$. Fully buckled systems can, however, be realized in systems with fixed boundaries preventing this collapse; in such systems, the fixed boundary imposes a stress σ satisfying eqn (12) that maintains the system at the threshold between the regimes of Fig. 2(c) and (d). This sets the amplification at the $R^* \to R$ limit of eqn (23):

$$\mathcal{A} = \left(1 + \frac{\lambda}{2\mu}\right)\frac{R}{R_0}, \tag{24}$$

and corresponds to the "density-controlled" regime of ref. 12.

Eqn (20)–(24) constitute a complete description of the active stress produced by the system as a function of the linear moduli and buckling stresses of the elastic medium, as well as the density and strength of the active units. These active stresses depend on the externally applied stress σ in the buckled regimes, as tensing the medium antagonizes buckling and amplification, which in turn decreases the active stress.

V. Constitutive relations

Constitutive stress–strain relations for the active material can be derived from eqn (20)–(24). Denoting the isotropic strain by $\gamma = u(R)/R$, we find that in the linear regime eqn (18) can be rewritten as

$$\sigma = (d\lambda + 2\mu)\gamma + \sigma_0\left(\frac{R_0}{R}\right)^d \tag{25a}$$

i.e., an affine stress–strain relation involving the same elastic modulus as for the passive system, consistent with the most common formulations of active gels theories. This linear regime is valid for large enough strains, namely

$$\gamma + \gamma_{\text{b}} > \frac{1-(R_0/R)^d}{\lambda + 2\mu}\frac{\sigma_0}{d}, \tag{25b}$$

where $\gamma_{\text{b}} = \sigma_{\text{b}}/(\lambda d + 2\mu)$ is the absolute value of the critical strain at which the elastic medium buckles in the absence of active units. At lower strains, the buckling regime of Fig. 2(b) takes over and yields a different stress–strain relation, albeit still an affine one:

$$\begin{aligned}\sigma = &\frac{2\mu(d-1)(d\lambda + 2\mu)\left[1-(R_0/R)^d\right]}{2\mu(d-1) + (d\lambda + 2\mu)(R_0/R)^d}\gamma \\ &+ \frac{d(\lambda + 2\mu)(R_0/R)^d}{2\mu(d-1) + (d\lambda + 2\mu)(R_0/R)^d}(\sigma_0 - \sigma_{\text{b}})\end{aligned} \tag{26a}$$

valid for strains

$$\left[\frac{1}{\lambda d + 2\mu} - \frac{(R_0/R)^d}{2\mu}\right]\frac{\sigma_0}{d} < \gamma + \gamma_{\text{b}} < \frac{1-(R_0/R)^d}{\lambda + 2\mu}\frac{\sigma_0}{d} \tag{26b}$$

Finally, for even lower (or more compressive) strains the buckling zone regime of Fig. 2(c) takes over, and the stress is nonlinearly related to the strain through

$$\sigma = (d\lambda + 2\mu)\gamma + \left(1 + \frac{\lambda}{2\mu}\right)\sigma_0 \frac{R_0^{d-1}R^*}{R^d}, \tag{27}$$

where R^* itself is a function of σ through eqn (14). Inserting eqn (27) into eqn (14) and defining

$$\tilde{\sigma} = \frac{\sigma + \sigma_{\text{b}}}{\sigma_0} \tag{28a}$$

$$\tilde{\gamma} = \frac{2\mu(\gamma + \gamma_{\text{b}})}{\sigma_0}, \tag{28b}$$

we get the following relation between stress and strain

$$\left[\tilde{\sigma} - \left(1 + \frac{d\lambda}{2\mu}\right)\tilde{\gamma}\right]^{d-1}[\tilde{\sigma} + (d-1)\tilde{\gamma}] = \frac{(1+\lambda/2\mu)^d}{1 + d\lambda/2\mu}\left(\frac{R_0}{R}\right)^{d(d-1)} \tag{29}$$

which is a polynomial equation of order d in σ and can be solved for σ in both $d = 2$ and $d = 3$. Here we present the more compact $d = 2$ result:

$$\tilde{\sigma} = \frac{\lambda\tilde{\gamma}}{\mu} + \left(1 + \frac{\lambda}{2\mu}\right)\sqrt{\frac{(R_0/R)^2}{1+\lambda/\mu} + \tilde{\gamma}^2}, \tag{30a}$$

and we give the bounds of this buckling zone regime in arbitrary dimension:

$$-\frac{\lambda(R_0/R)^{d-1}}{2\mu(d\lambda + 2\mu)}\sigma_0 < \gamma + \gamma_{\text{b}} < \left[\frac{1}{\lambda d + 2\mu} - \frac{(R_0/R)^d}{2\mu}\right]\frac{\sigma_0}{d}, \tag{30b}$$

where the lower bound of eqn (30b) represents the critical strain for the transition to the collapsed state of Fig. 2(d).

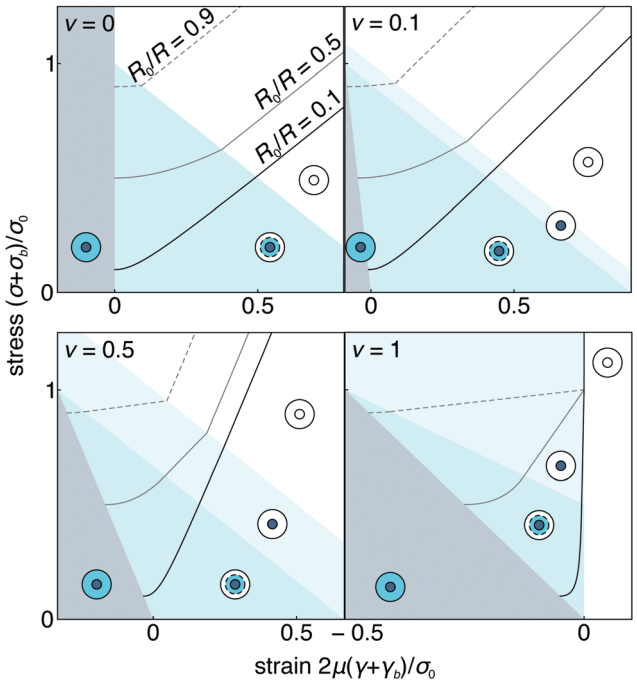

Fig. 5 Stress–strain relations for a $d = 2$ medium with embedded active units as a function of the Poisson ratio of the material (indicated in the top left corner of each panel) and the size of the active unit (see labeling of the lines in the top left panel). The colored regions denote the buckling regimes of Fig. 2. The slope of the stress–strain curves always vanishes as the system becomes unstable at the boundary of the collapsed (dark grey) regime.

Eqn (25)–(30) form a complete nonlinear constitutive relation relating the stress σ to the strain $\gamma = u(R)/R$ in elastic systems with embedded active units. We illustrate this relation in Fig. (5), which shows that the resulting active material always softens under compression before losing stability as the collapsing threshold is reached at low enough γ. In addition, the influence of the material's buckling threshold $\sigma_b = (d\lambda + 2\mu)\gamma_b$ and active unit stress σ_0 on this relation is remarkably simple, as they respectively result in a shift and a rescaling in the values of the stress and strain.

VI. Discussion

Active units embedded in fibrous media, such as molecular motors or whole contractile cells, exert strong forces on their surroundings. These active forces deform and buckle the fibers, thus affecting the way in which these forces are transmitted. Here we present a detailed analysis of this process and provide constitutive relations describing the material properties emerging from interactions between active unit and fiber networks. Such relations can readily be incorporated into macroscopic descriptions of active gels over short time scales ($\lesssim 100$ s[23]), where these gels are typically assumed to respond elastically.[19] Over longer times, fibers disentangle and detach, resulting in fluid-like network behavior. Nevertheless, if the time scale over which the active units detach from and reattach to the fibers ($\approx$ a few 100 ms[24]) is much shorter than that viscoelastic time scale, we expect active units to constantly pinch the network in alternating locations before it has time to flow, resulting in a state of constant tension well described by our predicted active stress. Now considering the microscopic length scale, our description could be supplemented with more detailed dynamical descriptions of the way in which the active unit stress σ_0 is produced[25,26] to elucidate the coupled dynamics of an active unit and its elastic environment.

Our present results show that buckling in fiber networks results in an amplification of active stress, consistent with the experimental measurements discussed in ref. 12. The buckling transitions underlying the force transmission described here proceed in several steps. The first step involves the buckling of the system's core shown in Fig. 2(b). This regime is clearly tied to our specific description of the active unit as a sphere of radius R_0, and may be substantially modified when using active units with different geometries. In the second buckling regime, a potentially large region surrounding of the active unit undergoes orthoradial buckling [Fig. 2(c)]. Contrary to the previous one, we expect this regime to be largely insensitive to the details of the active units, as the nonlinear response of fiber networks gives rise to an emergent isotropic force dipole away from the active units.[12] In the case of sparse active units $R_0 \ll R$, this regime occupies a much larger fraction of parameter space than the previous one (see Fig. 4), implying that its universal physics dominates nonlinear force transmission in systems with a low volume fraction of active units. Finally, the last transition considered here [Fig. 2(d)] corresponds to the limit of stability of the system, which cannot be described in a fixed stress ensemble. Indeed, the network does not have an intrinsic shape anymore, and collapses if its boundaries are released. However, at fixed boundary strain (*e.g.* for fixed or periodic boundary conditions), the system is characterized by a well-defined active stress, with an amplification factor proportional to R/R_0, as predicted numerically in our previous work.[12]

Our findings confirm and extend several heuristic conclusions formulated in our previous scaling arguments and numerical simulations of explicit filamentous networks.[12] While the model used in this previous work involves several realistic features not included in our current model, including a finite stiffness of the buckled network, fibers of varied lengths and the possibility of fiber alignment under force, our highly simplified continuum formalism captures the most important features of their behavior. We thus find that active stress amplification is rigorously proportional to the buckling radius R^*. We further provide a continuum counterpart to the "rope network" picture previously used to justify the r^{1-d} decay of stresses in the buckling zone, thus extending its relevance to non-fibrous materials. This anomalous stress decay has been observed experimentally[27] Finally, we find that the external stress σ influences stress amplification in an extremely simple way, as it enters the expressions characterizing the buckling thresholds, buckling radius and amplification factors only through the combination $\sigma + \sigma_b$, as illustrated in Fig. 1. More generally, the stress–strain relationship of the medium can be expressed as a relationship between $\sigma + \sigma_b$ and $\gamma + \sigma_b/(d\lambda + 2\mu)$ that does not explicitly depend on σ_b. In practice, this means that in the

fixed-stress ensemble the effect of prestressing the network is identical to that of shifting its buckling threshold σ_b by a quantity σ. In the fixed-strain ensemble, this implies that prestraining the network by γ is equivalent to shifting σ_b by $\sigma_{elastic} = (d\lambda + 2\mu)\gamma$.

The results derived in this paper are largely independent on the detailed characteristics of the elastic material considered, and are derived without the need of fully specifying a nonlinear stress–strain relation [see eqn (4)]. Indeed, our only nonlinear assumption is the plateauing of compressive stresses. Our study however leaves out elastic media with an auxetic linear response, *i.e.*, exotic materials whose lateral dimension shrinks when they are compressed vertically. Such materials undergo a different sequence of buckling transitions, which we discuss further in Appendix A. The characterization of these new regimes requires additional assumptions about the material's nonlinear properties, and generally do not yield closed-form expressions such as the ones presented here. Finally, our above discussion focuses on the case where $\sigma_b > 0$, *i.e.*, on materials that dramatically soften under compression. Our results are nonetheless formally applicable to materials with the opposite tendency, *e.g.* granular materials that lose all rigidity if their grains are pulled apart far enough to break the contacts between them. Indeed, simultaneously reversing the signs of all stresses, strains and displacements in our study converts the tense radial ropes underlying the force transmission in the $R_0 < r < R^*$ buckling zone of Fig. 2(c) into compressed granular columns with a similar propensity for long-range stress propagation. Whether such a state can be stable against the lateral buckling of such columns however remains to be determined.

Conflicts of interest

There are no conflicts to declare.

Appendix A: buckling transitions in auxetic materials

Here we outline the differences between the buckling scenarios associated with regular and auxetic ($\nu < 0$, or equivalently $\lambda < 0$) materials. First considering the linear regime, we compare the buckling thresholds associated with the inner and outer vicinity of the active unit by using eqn (9) to write

$$\begin{aligned}\sigma_{rr}(r < R_0) &= \sigma - \sigma_0 \frac{d\lambda + 2\mu + 2\mu(d-1)(R_0/R)^d}{d(\lambda + 2\mu)} \\ &= \sigma_{\theta\theta}(r < R_0), \qquad \text{(A1)} \\ \sigma_{\theta\theta}(R_0^+) &= \sigma - \sigma_0 \frac{2\mu + 2\mu(d-1)(R_0/R)^d}{d(\lambda + 2\mu)}\end{aligned}$$

Clearly, for auxetic materials we have $\sigma_{\theta\theta}(R_0^+) < \sigma_{rr}(r < R_0)$ and buckling occurs in the light blue annulus of Fig. 2(c) before it does in the dark blue circle of Fig. 2(b). Giving a detailed description of stress transmission in the medium beyond this threshold is a much more involved exercise than that presented in the main text of this article, as it requires giving a detailed description of the nonlinear stress–strain relation of the medium beyond eqn (4). Indeed, as the central region of the medium is still unbuckled, its stress can only be characterized by specifying the displacement of the medium at the inner rim of the light blue annulus, which thus requires a full characterization of displacements in the buckled region that the main text is able to avoid. Whether R^* reaches R before or after the central region starts to buckle strongly depends on that nonlinear stress–strain relation, yielding a less universal buckling scenario than the one observed for non-auxetic materials. We are not aware of the existence of any auxetic biological fiber network, nor do we feel confident enough to prescribe a detailed stress–strain relation for such a hypothetical material. We thus do not present a detailed investigation of auxetic materials here.

Acknowledgements

This work was supported by a PCTS fellowship to PR, the German Excellence Initiative *via* the program "NanoSystems Initiative Munich" (NIM) and the Deutsche Forschungsgemeinschaft (DFG) *via* the GRK2062/1 to CPB, Marie Curie Integration Grant PCIG12-GA-2012-334053, "Investissements d'Avenir" LabEx PALM (ANR-10-LABX-0039-PALM), ANR grant ANR-15-CE13-0004-03 and ERC Starting Grant 677532 to ML. ML's group belongs to the CNRS consortium CellTiss.

References

1 C. J. Jen and L. V. Mclntire, The Structural Properties and Contractile Force of a Clot, *Cell Motil.*, 1982, **2**, 445–455.
2 L. Blanchoin, R. Boujemaa-Paterski, C. Sykes and J. Plastino, Actin Dynamics, Architecture, and Mechanics in Cell Motility, *Physiol. Rev.*, 2014, **94**, 235–263.
3 C. P. Heisenberg and Y. Bellaïche, Forces in Tissue Morphogenesis and Patterning, *Cell*, 2013, **153**(5), 948–962.
4 C. P. Broedersz and F. C. MacKintosh, Modeling semiflexible polymer networks, *Rev. Mod. Phys.*, 2014, **86**, 995–1036.
5 M. E. Gurtin, in *Encyclopedia of Physics*, ed. S. Flügge, Springer-Verlag, 1972, vol. VIa/2, pp. 1–295.
6 P. Ronceray and M. Lenz, Connecting local active forces to macroscopic stress in elastic media, *Soft Matter*, 2015, **11**(8), 1597–1605.
7 Y. Shokef and S. A. Safran, Scaling Laws for the Response of Nonlinear Elastic Media with Implications for Cell Mechanics, *Phys. Rev. Lett.*, 2012, **108**(17), 178103.
8 H. Wang, A. S. Abhilash, C. S. Chen, R. G. Wells and V. B. Shenoy, Long-range force transmission in fibrous matrices enabled by tension-driven alignment of fibers, *Biophys. J.*, 2014, **107**(11), 2592–2603.
9 J. Notbohm, A. Lesman, P. Rosakis, D. A. Tirrell and G. Ravichandran, Microbuckling in fibrin networks enables long-range cell mechanosensing, *J. R. Soc., Interface*, 2015, **12**(108), 20150320.

10 P. Rosakis, J. Notbohm and G. Ravichandran, A model for compression-weakening materials and the elastic fields due to contractile cells, *J. Mech. Phys. Solids*, 2015, **85**, 16–32.
11 X. Xu and S. A. Safran, Nonlinearities of Biopolymer Gels Increase the Range of Force Transmission, *Phys. Rev. E: Stat., Nonlinear, Soft Matter Phys.*, 2015, **92**(03), 032728.
12 P. Ronceray, C. Broedersz and M. Lenz, Fiber networks amplify active stresses, *Proc. Natl. Acad. Sci. U. S. A.*, 2016, **113**(11), 2827–2832.
13 H. Wagner, Flat sheet metal girders with very thin metal web (Translated from German), *Z. Flugtechn. Motorl.*, 1929, **20**, 8–12.
14 A. C. Pipkin, The Relaxed Energy Density for Isotropic Elastic Membranes, *IMA J. Appl. Math.*, 1986, **36**, 85–99.
15 B. Davidovitch, R. D. Schroll, D. Vella, M. Adda-Bedia and E. A. Cerda, Prototypical model for tensional wrinkling in thin sheets, *Proc. Natl. Acad. Sci. U. S. A.*, 2011, **108**(45), 18227–18232.
16 K. Kruse, J. F. Joanny, F. Jülicher, J. Prost and K. Sekimoto, Generic theory of active polar gels: a paradigm for cytoskeletal dynamics, *Eur. Phys. J. E: Soft Matter Biol. Phys.*, 2005, **16**(1), 5–16.
17 F. Jülicher, K. Kruse, J. Prost and J. F. Joanny, Active behavior of the Cytoskeleton, *Phys. Rep.*, 2007, **449**(1–3), 3–28.
18 J. F. Joanny and J. Prost, Active gels as a description of the actin-myosin cytoskeleton, *HFSP J.*, 2009, **3**(2), 94–104.
19 J. Prost, F. Jülicher and J. F. Joanny, Active gel physics, *Nat. Phys.*, 2015, **11**(2), 111–117.
20 R. Voituriez, J. F. Joanny and J. Prost, Spontaneous flow transition in active polar gels, *Europhys. Lett.*, 2005, **70**(3), 404–410.
21 J. S. Bois, F. Jülicher and S. W. Grill, Pattern Formation in Active Fluids, *Phys. Rev. Lett.*, 2011, **106**(2), 028103.
22 K. V. Kumar, J. S. Bois, F. Jülicher and S. W. Grill, Pulsatory Patterns in Active Fluids, *Phys. Rev. Lett.*, 2014, **112**(20), 208101.
23 F. Wottawah, S. Schinkinger, B. Lincoln, R. Ananthakrishnan, M. Romeyke and J. Guck, *et al.*, Optical Rheology of Biological Cells, *Phys. Rev. Lett.*, 2005, **94**(9), 098103.
24 C. Veigel, J. E. Molloy, S. Schmitz and J. Kendrick-Jones, Load-dependent kinetics of force production by smooth muscle myosin measured with optical tweezers, *Nat. Cell Biol.*, 2003, **5**(11), 980–986.
25 C. E. Chan and D. J. Odde, Traction dynamics of filopodia on compliant substrates, *Science*, 2008, **322**(5908), 1687–1691.
26 M. Lenz, Geometrical Origins of Contractility in Disordered Actomyosin Networks, *Phys. Rev. X*, 2014, **4**, 041002.
27 Y. L. Han, P. Ronceray, G. Xu, A. Malandrino, R. D. Kamm, M. Lenz, C. P. Broedersz and M. Guo, Cell contraction induces long-ranged stress stiffening in the extracellular matrix, *Proc. Natl. Acad. Sci. U. S. A.*, 2018, **115**, 4075.

